

Breaking wave interaction with tandem cylinders under different impact scenarios

Hans Bihs ¹, Arun Kamath ² Mayilvahanan Alagan Chella³, and and Øivind A. Arntsen ⁴

1 ABSTRACT

2 The interaction of plunging breaking waves with a pair of cylinders placed in tandem is
3 investigated using the open-source computational fluid dynamics (CFD) model REEF3D.
4 The model is validated using experimental data for total wave forces and free surface for
5 breaking wave interaction with a single cylinder. Wave interaction with the tandem cylinders
6 is investigated for four different wave impact scenarios on the first cylinder and six different
7 distances between the cylinders in each scenario. The wave forces on the upstream cylinder
8 are generally found to be less than the force on a single cylinder for the particular scenario.
9 The force on the downstream cylinder is lower than the force on the upstream cylinder
10 when the breaker tongue impacts the first cylinder. Under conditions where the breaker
11 tongue impacts the downstream cylinder around the wave crest level, the wave force on the
12 downstream cylinder is higher than the force on the upstream cylinder. The wave forces
13 experienced by the tandem cylinders is highly influenced by the location of the breaking
14 point with respect to the cylinders and the distance between the cylinders.

15 **Keywords:** breaking wave forces, vertical cylinder, tandem cylinders, CFD, computational
16 fluid dynamics

¹Associate Professor, Dept. of Civil and Transport Engineering, Norwegian University of Science and Technology, Trondheim, 7491, Norway. E-mail: hans.bihs@ntnu.no

²Post Doctoral Fellow, Dept. of Civil and Transport Engineering, Norwegian University of Science and Technology, Trondheim, 7491, Norway.

³PhD candidate, Dept. of Civil and Transport Engineering, Norwegian University of Science and Technology, Trondheim, 7491, Norway

⁴Associate Professor, Dept. of Civil and Transport Engineering, Norwegian University of Science and Technology, Trondheim, 7491, Norway.

17 INTRODUCTION

18 The interaction of breaking wave forces on structures involves complex two-phase air-
19 water interaction, rapid free surface deformations and an impulsive force. The short duration
20 over which these interactions occur, pose several challenges to the evaluation of breaking wave
21 forces. In shallow waters, the hydrodynamic loading on structures such as offshore wind
22 turbine substructures is mostly governed by the loading due to plunging breaking waves
23 (Alagan Chella et al., 2012). The theoretical description of breaking waves in shallow waters
24 is rather limited up to the transition region close to breaking. The evolution of breaking
25 process and the underlying flow physics can not be described theoretically. This is due to the
26 simplifying assumptions of single-phase and two-dimensional flow, irrotational motion, no
27 return flow and hydrostatic pressure made in obtaining analytical solutions (Cokelet, 1977).

28 The current knowledge on breaking wave kinematics are mainly based on experimental
29 investigations. In current literature, studies for deep water breaking waves by Kjeldsen and
30 Myrhaug (1978); Battjes and Sakai (1981); Bonmarin (1989); Rapp and Melville (1990) and
31 Duncan (2001); studies for wave breaking on plane beaches by Stive and Wind (1982); Miller
32 (1987); Nadaoka et al. (1989) and Ting and Kim (1994) and for wave breaking over submerged
33 structures by Gourlay (1994); Smith and Kraus (1990) and Blenkinsopp and Chaplin (2008)
34 are notable. While these studies focussed on the kinematics and dynamics of breaking waves,
35 several other researchers experimentally investigated breaking wave forces on cylinders such
36 as Goda et al. (1966); Watanbe and Horikawa (1974); Apelt and Piorewicz (1986); Chan and
37 Melville (1988); Sawaragi and Nochino (1984); Chaplin et al. (1992); Wienke et al. (2000)
38 and Arntsen et al. (2011). However, the measurement of the quantities related to the wave
39 breaking and their interaction with structures are challenging.

40 Theoretically, the total breaking wave force on a vertical slender cylinder can be expressed
41 in terms of a slowly varying quasi-static force and the impulsive wave impact force. Goda
42 et al. (1966) proposed the use of an impact force term in addition to the quasi-static force
43 predicted by the Morison formula (Morison et al., 1950) to evaluate breaking wave forces.

44 The impact force characteristics are mainly determined by the geometric properties and
45 kinematics at breaking such as the shape of the wave and the distribution of water particle
46 velocities under the wave crest (Goda et al., 1966).

47 Watanabe and Horikawa (1974) investigated breaking wave forces on a large cylinder and
48 proposed a formula including the phase difference between the water particle acceleration
49 and the inertia force. They also pointed out that empirical coefficients used to calculate
50 the breaking wave forces are not universal and depend on the breaking wave characteristics.
51 Apelt and Piorewicz (1986) carried out experiments to study the interference effects on
52 breaking wave forces on a row of two and three vertical cylinders placed along and normal to
53 the direction of wave propagation. Their results suggested that both the distance between
54 the cylinders and incident wave steepness are important factors when in the row is arranged
55 normal to the direction of wave propagation. They further concluded that the distance of
56 separation does not have a significant influence on the wave forces when the row is along the
57 direction of wave propagation. Sparboom et al. (2005) studied breaking wave forces on two
58 and three cylinder arrays due to freak waves and found that the breaking wave forces are
59 reduced significantly along the array due to the sheltering effect from the upstream cylinders.

60 Wienke et al. (2000) carried out large-scale studies on breaking wave impact on a single
61 slender cylinder and presented different wave loading cases, considering the position of the
62 cylinder with respect to the wave breaking point. Irschik et al. (2002) extended this work
63 and presented the Empirical Mode Decomposition (EMD) method to separate the slowly
64 varying quasi-static loading and the dynamic response of the cylinder from the measured
65 breaking wave force history. Wienke and Oumeraci (2005) proposed a theoretical model to
66 calculate breaking wave forces on a single slender cylinder using the wave celerity and the
67 curling factor as inputs based on their large-scale investigations.

68 The curling factor (λ) is a parameter used to determine the contribution of the wave crest
69 to the wave impact force during breaking wave impact. The values for λ are determined
70 experimentally for different bottom slopes and water depths and these values depend on

71 the breaker type. According to Wienke and Oumeraci (2005), the wave impact scenario
72 for different distances of the cylinder surface from the breaking point is different. The
73 assumption of instantaneous impact of the wave on the cylinder while calculating λ can
74 also lead to overestimation of the breaking wave force. Hildebrandt and Schlurmann (2012)
75 investigated breaking wave forces on a tripod structure in large-scale experiments to study
76 the detailed temporal and spatial variation in the wave slamming loads. They concluded
77 that the curling factors, vertical position of impact and the maximum slamming coefficients
78 increase with decreasing distance between the cylinder from the point of wave breaking.
79 Their results agreed with the theoretical slamming coefficients given by Goda et al. (1966).

80 Most of the current approaches to evaluate breaking wave forces strongly depend on the
81 experimentally determined coefficients. However, the measurement of the various parame-
82 ters such as velocity and acceleration during breaking is a challenging task (Arntsen et al.,
83 2011). Also, these methods are not valid for cases which are not similar to the experiments
84 used to obtain the coefficients and cannot be applied for multiple cylinders and different
85 arrangements of the cylinders. In addition, the distance of the cylinder from the breaking
86 point results in several breaking wave interaction scenarios that have to be studied in detail
87 to gain useful insights into the breaking wave-structure interaction problem.

88 Numerical modeling of breaking waves requires the evaluation of the fluid physics with few
89 assumptions as carried out using computational fluid dynamics (CFD) models (Christensen,
90 1998) in order to obtain detailed insights into the breaking wave-structure interaction. Many
91 numerical studies have been carried out to investigate the breaking process in shallow waters
92 with single-phase CFD models (Lin and Liu, 1998; Bradford, 2000; Christensen and Deigaard,
93 2001; Zhao et al., 2004). Hieu et al. (2004) showed that a two-phase CFD model better
94 resolves the breaking wave kinematics. Thus, two-phase CFD models are generally used
95 in recent literature to include the air-water interaction in the modeling (Chen et al., 1999;
96 Christensen, 2006; Wang et al., 2009; Jacobsen et al., 2012; Xie, 2013; Alagan Chella et al.,
97 2015b). In addition, results from Alagan Chella et al. (2015b) and Alagan Chella et al.

98 (2015a) show that higher order discretization schemes, a tight velocity-pressure coupling
99 and a sharp representation of the free surface provide a more realistic description of the
100 breaking waves. These studies have advanced the knowledge in current literature regarding
101 breaking wave kinematics.

102 Bredmose and Jacobsen (2010) carried out simulations of focussed wave breaking forces
103 on a slender cylinder using the open-source CFD model OpenFOAM, without an explicit
104 turbulence model with half of the computational domain and assuming lateral symmetry
105 in the flow field. Mo et al. (2013) investigated solitary wave breaking and its interaction
106 with a slender cylinder over a slope with a CFD model assuming lateral symmetry and also
107 with experiments. Good agreement between the experimental and numerical results is found
108 for the free surface elevations and particle velocities. Choi et al. (2015) studied the free
109 surface elevation and breaking wave forces on a vertical and inclined single cylinders using a
110 CFD model. A good agreement was obtained between the computed results and the filtered
111 experimental data. However, numerical investigation of breaking wave forces on tandem
112 cylinders, the effect of neighboring cylinders on the breaking wave forces, along with the
113 complex free surface deformations associated with the interaction has not been presented in
114 current literature to the knowledge of the authors.

115 The interaction of breaking waves with a cylinder involves several important free surface
116 features such as runup on the cylinder, the separation of the breaking wavefront around
117 the cylinder, formation of a water jet behind the cylinder and the rejoining of the separated
118 wavefront behind the cylinder. The scenario is further relevant in the presence of neighboring
119 cylinders, as is the case in coastal and offshore constructions. In this study, the open-source
120 CFD model REEF3D is used to evaluate breaking wave forces on tandem cylinders placed at
121 different distances from each other in a three-dimensional numerical wave tank. The model
122 has been previously used to investigate the breaking wave kinematics (Alagan Chella et al.,
123 2015b) and to calculate non-breaking wave forces on tandem cylinders (Kamath et al., 2015).
124 Several free surface free features and wave impact scenarios associated with breaking wave

125 interaction with a single cylinder and the consequences on the wave forces acting on the
 126 cylinder have been discussed in current literature. This paper investigates the case of two
 127 cylinders placed in tandem with focus on the influence of the distance of separation between
 128 the cylinders on the wave forces along with the consequences of the flow features associated
 129 with breaking wave interaction with the cylinders. Four different wave impact scenarios on
 130 the first cylinder and six distances of separation between the cylinders are considered. The
 131 numerical model is validated using experimental results from the Large Wave Flume (GWK)
 132 (Irschik et al., 2002) for breaking wave interaction with a single cylinder.

133 NUMERICAL MODEL

134 Governing equations

135 The numerical wave tank REEF3D solves the incompressible three-dimensional Reynolds-
 136 Averaged Navier-Stokes (RANS) equations:

$$137 \quad \frac{\partial u_i}{\partial x_i} = 0 \quad (1)$$

$$138 \quad \frac{\partial u_i}{\partial t} + u_j \frac{\partial u_i}{\partial x_j} = -\frac{1}{\rho} \frac{\partial p}{\partial x_i} + \frac{\partial}{\partial x_j} \left[(\nu + \nu_t) \left(\frac{\partial u_i}{\partial x_j} + \frac{\partial u_j}{\partial x_i} \right) \right] + g_i \quad (2)$$

139 where u is the velocity, ρ is the density of the fluid, p is the pressure, ν is the kinematic
 140 viscosity, ν_t is the eddy viscosity and g the acceleration due to gravity.

141 The fifth-order conservative finite difference Weighted Essentially Non-Oscillatory (WENO)
 142 scheme proposed by Jiang and Shu (1996) is applied for the discretization of the convective
 143 terms of the RANS equation. Time advancement is carried out using a Total Variation
 144 Diminishing (TVD) third-order Runge-Kutta explicit time scheme (Shu and Osher, 1988).
 145 The time step size is controlled with adaptive time stepping based on the CFL criterion.
 146 This results in an optimal time step value for numerical stability and accuracy. The diffu-
 147 sion is treated with an implicit time scheme in order to exclude it from the CFL criterion.
 148 The pressure is treated with the projection method (Chorin, 1968). The Poisson equation

149 for the pressure is solved with the preconditioned BiCGStab solver (van der Vorst, 1992).
 150 The domain decomposition strategy and MPI (Message Passing Interface) is used for paral-
 151 lelization. A Cartesian grid with a staggered arrangement is used in the numerical model.
 152 Complex geometries are taken into account with the ghost cell immersed boundary method
 153 (Berthelsen and Faltinsen, 2008).

154 The k - ω model is employed for turbulence closure (Wilcox, 1994) with transport equations
 155 for the turbulent kinetic energy k and the specific turbulence dissipation ω shown in Eq. (3)
 156 and (4) respectively. Wall functions are used for k and ω .

$$157 \quad \frac{\partial k}{\partial t} + u_j \frac{\partial k}{\partial x_j} = \frac{\partial}{\partial x_j} \left[\left(\nu + \frac{\nu_t}{\sigma_k} \right) \frac{\partial k}{\partial x_j} \right] + P_k - \beta_k k \omega \quad (3)$$

$$158 \quad \frac{\partial \omega}{\partial t} + u_j \frac{\partial \omega}{\partial x_j} = \frac{\partial}{\partial x_j} \left[\left(\nu + \frac{\nu_t}{\sigma_\omega} \right) \frac{\partial \omega}{\partial x_j} \right] + \frac{\omega}{k} \alpha P_k - \beta \omega^2 \quad (4)$$

160 where, eddy viscosity $\nu_t = k/\omega$, P_k is the production rate and closure coefficients $\sigma_k = 2$,
 161 $\sigma_\omega = 2$, $\alpha = 5/9$, $\beta_k = 9/100$, $\beta = 3/40$. Eddy viscosity limiters (Durbin, 2009) are used
 162 to control the overproduction of turbulence, often occurring in highly unsteady free surface
 163 flows. In addition, the fact that the turbulence length scales cannot pass the interface
 164 between water and air is considered with a free surface turbulence damping scheme (Naot
 165 and Rodi, 1982).

166 Free Surface

167 The complex wave hydrodynamics are modeled with a two-phase flow approach, calculat-
 168 ing the flow for water and air. The interface between the two fluids is captured with the level
 169 set method (Osher and Sethian, 1988). The zero level set of the signed distance function
 170 $\phi(\vec{x}, t)$ represents the location of the free surface. With its signed distance property, it gives
 171 the shortest distance from the interface to all the points in the flow domain. Based on the

172 sign of the level set function, the phases can be distinguished as follows:

$$173 \quad \phi(\vec{x}, t) \begin{cases} > 0 & \text{if } \vec{x} \text{ is in phase 1} \\ = 0 & \text{if } \vec{x} \text{ is at the interface} \\ < 0 & \text{if } \vec{x} \text{ is in phase 2} \end{cases} \quad (5)$$

174 The flow velocities calculated from Eq. (2) are used to convect the level set function:

$$175 \quad \frac{\partial \phi}{\partial t} + u_j \frac{\partial \phi}{\partial x_j} = 0 \quad (6)$$

176 During the computation, reinitialization is carried out after every iteration using a partial
 177 differential equation Peng et al. (1999) in order to maintain the signed distance property
 178 of the level set function. The level set function is discretized with the Hamilton-Jacobi
 179 formulation of the WENO scheme by Jiang and Peng (2000)

180 **Wave generation and absorption**

181 The numerical wave tank uses the relaxation method (Larsen and Dancy, 1983) for the
 182 wave generation. A relaxation function is used to moderate the velocity and the free surface
 183 using a wave theory in the relaxation zones with Eq. (7):

$$184 \quad u_{relaxed} = \Gamma(x)u_{analytical} + (1 - \Gamma(x))u_{computational} \quad (7)$$

$$185 \quad \phi_{relaxed} = \Gamma(x)\phi_{analytical} + (1 - \Gamma(x))\phi_{computational}$$

186 where $\Gamma(x)$ is the relaxation function and $x \in [0, 1]$ is the x -coordinate scaled to the length
 187 of the relaxation zone. The relaxation function shown in Eq. (8) is used in the current
 188 numerical model (Jacobsen et al., 2012):

$$189 \quad \Gamma(x) = 1 - \frac{e^{(1-x)^{3.5}} - 1}{e - 1} \quad (8)$$

190 In order to avoid reflections from the downstream boundary, an active wave absorption

191 method is employed. Here, waves opposite to the reflected ones are generated, canceling out
 192 the reflections. Based on shallow water theory (Schäffer and Klopman, 2000), the following
 193 horizontal velocity is prescribed on the downstream boundary:

$$194 \quad u(t) = -\sqrt{\frac{g}{h}} \xi(t) \quad (9)$$

195 where

$$196 \quad \xi(t) = \eta(t) - h \quad (10)$$

197 Here, $\eta(t)$ is the actual free surface location along the downstream boundary and h the
 198 still water level. The method is applied in vertical strips along the downstream boundary,
 199 which are one grid cell wide. This way, different free surface elevations along the boundary
 200 can be taken into account (Higuera et al., 2013). Also, the handling of oblique waves is also
 201 implemented in the current model.

202 Numerical evaluation of wave forces

203 The breaking wave forces on the cylinders is calculated by integrating the pressure p and
 204 the surface normal component of the viscous shear stress tensor τ on the surface of the solid
 205 objects:

$$206 \quad F = \int_{\Omega} (-\mathbf{n}p + \mathbf{n} \cdot \tau) d\Omega \quad (11)$$

207 where \mathbf{n} is the unit normal vector pointing into the fluid and Ω is the surface of the object.

208

209 RESULTS AND DISCUSSION

210 Validation of the numerical model

211 The breaking wave force on a single vertical cylinder is calculated numerically and com-
 212 pared to experimental data to validate the numerical model. The experiments were carried
 213 out at the Large Wave Flume (GWK), Hannover, Germany (Irschik et al., 2002) on a vertical
 214 cylinder of diameter $D = 0.7$ m in a water depth of 3.80 m with incident waves of period

215 $T = 4.0$ s. The cylinder is placed at the top of a 23 m long 1 : 10 slope, such that the still
216 water depth at the cylinder is 1.50 m. In the numerical setup, the wave tank is 59 m long,
217 5 m wide and 7 m high with a grid size of $dx = 0.05$ m resulting in a total of 16.52 million
218 cells. A cylinder with $D = 0.7$ m is placed with its center at 44.0 m and the incident waves of
219 period $T = 4.0$ s break exactly on the front surface of the cylinder. The complete numerical
220 setup is illustrated in Fig. (1a). The definition sketch for tandem cylinders in the wave tank
221 showing the location of the wave gages and the separation distance is shown in Fig. (1b).

222 The numerically calculated wave force is compared to the EMD (Empirical Mode De-
223 composition) treated experimental data from Choi et al. (2015) to filter out the dynamic
224 amplification of the wave forces due to the vibration of the cylinder in Fig. (2a). A good
225 agreement is seen between the numerical and experimental wave forces. The numerical re-
226 sults are also similar over several wave periods, showing that the numerical model predicts the
227 the wave breaking location and consequently the breaking wave forces consistently. The free
228 surface elevation near the wall along the frontline of the cylinder provides a representation
229 of the wave incident on the cylinder. The comparison between numerical and experimental
230 free surface elevation shows a good agreement in Fig. (2b). The vertical wavefront in the
231 figure shows that the wave breaks on the front surface of the cylinder.

232 **Effect of wave impact scenario and distance between tandem cylinders on the** 233 **wave forces**

234 The wave forces on tandem cylinders placed at different distances from each other are
235 studied for different wave breaking scenarios. The different scenarios are determined based
236 on the location of the wave breaking point with respect to the front surface of the first
237 cylinder. The scenarios considered in this study are:

- 238 ● scenario A: overturning wave crest impacts cylinder 1 just below the wave crest level
- 239 ● scenario B: overturning wave crest impacts cylinder 1 at the wave crest level
- 240 ● scenario C: wave breaks exactly at cylinder 1 with a vertical wavefront

241 • scenario D: wave breaks just behind cylinder 1

242 The various scenarios are illustrated in Fig. (3). Simulations are carried out to determine
243 the breaking wave force for a single cylinder, F_0 in each of the scenarios. Previous studies
244 dealing with breaking wave interaction with a single slender cylinder have presented that
245 the mode of wave impact on the cylinder due to the distance between the breaking point
246 and the location of the cylinder have a significant impact on the wave forces acting on it.
247 According to Irschik et al. (2002), scenario A and B result in the highest and the second
248 highest total wave forces on a single cylinder respectively. The lowest wave forces on a single
249 cylinder are obtained in scenario D. In the context of tandem cylinders, the wave impact on
250 cylinder 1 and the separation distance between the two cylinders can play an important role
251 in the wave forces experienced by both the cylinders. This is investigated in this study by
252 placing the second cylinder at separation distances of $S = 1D$, $S = 2D$, $S = 3D$, $S = 4D$,
253 $S = 5D$ and $S = 6D$ from the first cylinder. The resulting 24 different cases are listed in
254 Table (1) along with the numerical force calculated for a single cylinder in each of the wave
255 breaking scenarios, F_0 , the maximum force on each cylinder with respect to F_0 in each case
256 (F_1/F_0 and F_2/F_0) and the maximum wave crest elevations in front of the cylinders with
257 respect to the incident wave crest elevation $\eta_0 = 0.789$ m (η_{cyl1}/η_0 and η_{cyl2}/η_0). In the
258 following sections, results from selected cases are presented to obtain detailed insights into
259 the breaking wave interaction, free surface features and the wave forces on the cylinders. The
260 selected cases present the prominent breaking wave hydrodynamics for different separation
261 distances in the different wave impact scenarios.

262 *Scenario A1: overturning wave crest impacting cylinder 1 just below the wave crest level with*
263 *$S = 1D$*

264 The breaking wave force and the free surface elevations around the cylinders calculated
265 for scenario A1 are presented in Fig. (4). The breaking wave force on a single cylinder in this
266 wave impact scenario is $F_0 = 14000$ N. The breaking wave force (F) on cylinder 1 and 2 are

267 calculated to be $0.92F_0$ and $0.59F_0$ respectively in Fig. (4a). In this case, the wave incident
 268 on the second cylinder is a broken wave that has dissipated most of its energy in the breaking
 269 process and during its interaction with the first cylinder. Thus, the breaking wave force on
 270 the second cylinder is significantly lower than that on the first cylinder. The free surface
 271 elevations (η) calculated in front (WG 1) and behind (WG 2) the first cylinder and in front
 272 of the second cylinder (WG 3) are presented in Fig. (4b). The free surface elevation in front
 273 of cylinder 2, placed $S = 1D$ away is $\eta/\eta_0 = 1.69$, higher than the free surface elevation in
 274 front of cylinder 1, $\eta/\eta_0 = 1.58$. The higher free surface elevation is attributed to the large
 275 runup on cylinder 2 due to the close placement of the cylinders.

276 Further insight into the wave interaction problem is obtained from the free surface around
 277 the cylinders for case A1, presented in Fig. (5) with horizontal velocity contours. The incident
 278 wave impacts cylinder 1 with the breaker tongue just below the wave crest level in Fig. (5a).
 279 The overturned wavefront is separated around cylinder 1 in Fig. (5b). This phenomenon
 280 of separation of the wave crest around the first cylinder and spreading of the water mass
 281 around the sides of the cylinder is also reported by Sparboom et al. (2006) in large-scale
 282 experiments investigating breaking wave interaction with slender cylinders. Figure (5c)
 283 shows the separated broken wavefront incident on cylinder 2 and reconnecting with the free
 284 surface. As the broken wave crest propagates past cylinder 2 in Fig. (5d), the high runup
 285 on the front surface of cylinder 2 is observed. This runup results in a higher free surface
 286 elevation in front of cylinder 2 compared to cylinder 1 seen for WG 3 in Fig. (4b). Figure
 287 (5) also shows that in scenario A, cylinder 2 is always exposed to an already broken wave,
 288 due to which the cylinder experiences lower wave forces.

289 *Scenario B2: overturning wave crest impacting cylinder 1 at the wave crest level with $S = 2D$*

290 Figure (6) shows the breaking wave forces on and the free surface elevations around the
 291 two cylinders in scenario B2. A single cylinder in the same impact scenario experiences a
 292 forces of $F_0 = 13400$ N. The breaking wave force on cylinder 1 is $0.93F_0$ and on cylinder 2
 293 it is $0.85F_0$, shown in Fig.(6a). The free surface elevations in front of cylinders 1 and 2 in

294 Fig. (6b) are $\eta/\eta_0 = 1.70$ and $\eta/\eta_0 = 1.72$ respectively. The slopes of the wavefront at the
295 moment of impact on the cylinders are similar and the wave forces on the two cylinders are
296 comparably similar.

297 The free surface around the cylinders in scenario B2 with horizontal velocity contours
298 is shown in Fig. (7). The overturning wave crest impacts cylinder 1 at wave crest level
299 in Fig. (7a). The waves reflected by the cylinders from the previous wave impact is seen
300 interacting with the incident wave crest. The separation of the overturning wave crest around
301 cylinder 1 is seen in Fig. (7b). The overturning wave crest impacts cylinder 2 below wave
302 crest level along with the water jet formed behind the first cylinder in Fig. (7c). The high
303 runup on the second cylinder due to the water jet originating behind cylinder 1 and the
304 small separation distance is seen in Fig. (7d). In this scenario, though cylinder 1 separates
305 the wavefront, the sheltering effect on cylinder 2 is seen to be reduced. This is due to water
306 jet formed behind cylinder 1 that impacts cylinder 2 along with the breaking wave. This
307 results in comparably similar forces on the two cylinders in this scenario, with the upstream
308 cylinder experiencing a slightly higher force.

309 *Scenario C3: wave breaking exactly at cylinder 1 with $S = 3D$*

310 The breaking wave forces on and the free surface elevations around the cylinders in
311 scenario C3 are shown in Fig. (8). The breaking wave force on a single cylinder in this
312 scenario is $F_0 = 11850$ N. Here, cylinder 1 experiences a force of $0.92F_0$ and cylinder 2 a
313 force of $0.97F_0$. It is observed that the breaking wave force on the downstream cylinder 2 is
314 slightly higher than the force on the upstream cylinder 1. The free surface elevation in front
315 of cylinder 2 is $\eta/\eta_0 = 1.70$, slightly lower compared to $\eta/\eta_0 = 1.82$ in front of cylinder 1.

316 The wave interaction in scenario C3 is further studied using the free surface around the
317 cylinders with horizontal velocity contours in Fig. (9). The incident wave impacting cylinder
318 1 with a vertical wavefront is seen in Fig. (9a). The incident wave is separated around
319 cylinder 1 in Fig. (9b) and the wave crest also begins to overturn just behind the cylinder.
320 The breaker tongue impacts cylinder 2 along with the water jet originating behind cylinder

321 1 in Fig. (9c). The breaking wave incident on cylinder 2 impacts the cylinder just below the
322 wave crest level along with the water jet, justifying the higher forces on the cylinder. The
323 runup of the trapped water between the cylinders is seen in Fig. (9d) and the overturning
324 wave crest rejoins the preceding wave crest after passing cylinder 2.

325 *Scenario D4: wave breaking just behind cylinder 1 with $S = 4D$*

326 The waves force on a single cylinder in this wave impact scenario is calculated to be
327 $F_0 = 9800$ N. In Fig. (10a), the calculated breaking wave forces on cylinder 1 and 2 are
328 $0.88F_0$ and $1.04F_0$ respectively. In this scenario, the upstream cylinder 1 is exposed to very
329 steep incident waves approaching the wave breaking point. Cylinder 2 is exposed to an
330 overturning wave crest and the breaking wave impact force contributes to the total wave
331 force on the cylinder, resulting in a higher wave force on the downstream cylinder compared
332 to the upstream cylinder. The free surface elevations in Fig. (10b) show that $\eta/\eta_0 = 1.78$ in
333 front of cylinder 1 (WG 1) and higher than $\eta/\eta_0 = 1.59$ in front of cylinder 2 (WG 3) in this
334 case.

335 In order to further understand the wave interaction with the cylinders in scenario D4,
336 the free surface around the cylinders is presented in Fig. (11) along with horizontal velocity
337 contours. Figure (11a) shows the steep unbroken wave incident on cylinder 1. The wave
338 breaks just behind cylinder 1 and the overturning wave crest along with the water jet origi-
339 nating behind cylinder 1 is seen in Fig. (11b). The overturning wave crest then impacts the
340 second cylinder just below the wave crest level in Fig. (11c) along with the water jet. The
341 breaker tongue reconnects with the preceding wave trough behind cylinder 2 in Fig. (11d).
342 The higher forces on the second cylinder are justified by the mode of wave impact on each
343 cylinder. Figure (11) clearly shows that the upstream cylinder 1 is exposed to a steep non-
344 breaking wave, whereas the overturning wave crest impacts the downstream cylinder 2 just
345 below the wave crest level.

346 *Scenario D6: wave breaking just behind cylinder 1 with $S = 6D$*

347 The wave forces on the cylinders 1 and 2 in this case are calculated to be $0.85F_0$ and
348 $1.03F_0$ respectively in Fig. (12a). The wave force on the cylinder 2 is significantly higher
349 than the force on cylinder 1 in this scenario. The free surface elevation in front of cylinder
350 1, $\eta/\eta_0 = 1.78$ is higher than the free surface in front of cylinder 2 which is $\eta/\eta_0 = 1.37$ in
351 Fig. (12b). The breaking wave impact on cylinder 2 is represented by the steep front face
352 of the wave in front of the cylinder during the same time as the peak force on the cylinder.
353 The runup on cylinder 2 is seen to lesser in this scenario ($\eta/\eta_0 = 1.37$) compared to scenario
354 D4 ($\eta/\eta_0 = 1.59$).

355 The free surface around the cylinders along with the horizontal velocity contours is pre-
356 sented in Fig. (13). The steep unbroken wave incident on cylinder 1 is seen in Fig. (13a),
357 similar to that in Fig. (11a). Figure (13b) shows the overturning crest and the water jet
358 originating behind cylinder 1 in between the two cylinders. The impact of the water jet on
359 cylinder 2 after the overturning wave crest has impacted the cylinder is seen in Fig. (13c).
360 The runup on cylinder 2 in this scenario is lower due to the longer separation distance be-
361 tween the cylinders. The overturning wave crest and the water jet impact the cylinder close
362 to the point of reconnection of the breaking wave crest with the preceding wave trough. The
363 broken wave and the water jet formed behind cylinder 2 are seen in Fig. (13d).

364 **Variation of the breaking wave forces on the cylinders with separation distance** 365 **in the different wave impact scenarios**

366 The variation of the total breaking wave forces on each of the cylinders in the different
367 wave impact scenarios for different separation distances is presented in Fig. (14). The fol-
368 lowing sections correlate the variation of the forces with the separation distance with the
369 free surface features associated with the wave impact scenario.

370 *Scenario A*

371 The total wave force on cylinder varies over a small range between $0.95F_0$ - $0.88F_0$ for
372 scenario A in Fig. (14a). For cylinder 2, the total wave force varies significantly with a

373 lowest of $0.45F_0$ for $S = 3D$ to a highest of $0.59F_0$ for $S = 1D$. Cylinder 2 is always exposed
 374 to a broken wave and the water jet originating behind cylinder 1, along with the free surface
 375 features behind cylinder 1 have a significant effect on the total wave force on cylinder 2. For
 376 small separation distances of $S = 1D$ and $2D$, a separated broken wave crest is incident on
 377 cylinder 2 as seen in Fig. (5c). The water jet originating behind cylinder 1, that develops
 378 in the small region between the cylinders is mainly responsible for the force on cylinder 2.
 379 The resulting forces for $S = 1D$ and $2D$ are seen to be around $0.58F_0$ in Fig. (14a). On
 380 increasing the distance to $S = 3D$, the force resulting from the impact of the water jet is
 381 reduced and the minimum force is calculated for this scenario. On further increasing the
 382 separation distance to $S = 4D$ and $5D$, the wave crest separated by cylinder 1 rejoins the
 383 preceding wave trough, undergoes secondary breaking and impacts cylinder 2 along with the
 384 water jet. This results in the slightly increasing trend in the force on cylinder 2. For $S = 6D$,
 385 cylinder 2 is mainly exposed to the post-breaking splash up and the force on cylinder 2 is
 386 lowered again. Further increase in the separation distance S would result in further reduction
 387 on the wave force on cylinder 2.

388 *Scenario B*

389 The total wave forces on both cylinders are significantly affected by the separation dis-
 390 tance between the cylinders in this scenario as seen in Fig. (14b). The total wave force on
 391 cylinder 1 is highest for $S = 2D$ with $0.93F_0$ and lowest for $S = 3D$ with $0.61F_0$. For cylin-
 392 der 2, the total wave force is a maximum of $0.85F_0$ for $S = 2D$ and a minimum of $0.57F_0$
 393 for $S = 4D$. In this case, the waves reflected from the cylinders interact with the incident
 394 overturning wave crest as seen in Fig. (7a). This results in significant changes in wave forces
 395 on both cylinders as the separation distance between the cylinders is varied. When $S = 1D$,
 396 the incident wave is separated by cylinder 1 and cylinder 2 is impacted mainly by the water
 397 jet. This results in lower forces on cylinder 2. As S is increased to $2D$, the separated wave
 398 crest is rejoined just before impacting cylinder 2 and the force on the cylinder increases.
 399 The interaction between the incident wave crest and the reflected waves from the cylinders

400 for $S = 3D$ result in reduced forces on cylinder 1. At the same time, the wave incident on
 401 cylinder 2 rejoins the preceding wave trough just in front of the cylinder and the force on
 402 the cylinder is reduced, but is higher than the force on cylinder 1. Further increase in S
 403 results in lower forces on cylinder 2, since the incident wave has rejoined the preceding wave
 404 trough and the cylinder is exposed the splash up. The forces on cylinder 1 increase and
 405 reach around the value calculated for $S = 1D$ following the interaction between the incident
 406 and reflected waves. Hildebrandt et al. (2008) found through large-scale experiments with
 407 non-breaking waves on groups of slender cylinders that for certain distances of separation,
 408 the forces on the upstream cylinder are influenced by the wave interaction between the cylin-
 409 ders and waves reflected by the cylinders. Their observations are applicable in this case with
 410 a strong interaction between the incident wave and the reflected waves from the cylinders
 411 when the overturning wave crest impacts cylinder 1 at wave crest level.

412 *Scenario C*

413 In scenario C the front surface of cylinder 1 is at the wave breaking point and the peak
 414 breaking wave force on the cylinder varies between $0.92F_0$ ($S = 3D$) and $0.83F_0$ ($S = 6D$)
 415 in Fig. (14c). The peak wave force on cylinder 2 varies significantly with the separation
 416 distance with a maximum of $0.97F_0$ for $S = 3D$ and a minimum of $S = 0.61F_0$ for $S = 6D$.
 417 It is seen that for $S = 3D$ and $4D$, the breaking wave force on the downstream cylinder 2
 418 is slightly higher than the upstream cylinder 1. The variation of the forces on cylinder 2
 419 can be justified by the wave breaking process in this scenario and the resulting free surface
 420 features seen between the cylinders. For $S = 1D$, the incident wave is separated by cylinder
 421 1 and the water jet originating behind the cylinder impacts cylinder 2 leading to a lower
 422 force on the cylinder. The separated wave crest rejoins before impacting cylinder 2, along
 423 with the water jet when $S = 2D$ and the wave force is increased. On further increasing S to
 424 $3D$ and $4D$, the breaker tongue impacts the cylinder around the wave crest level along with
 425 the water jet as seen in Fig. (9c), resulting in a higher force on cylinder 2 than on cylinder
 426 1. For $S = 5D$ and $6D$, cylinder 2 is exposed mainly to the splash up along with the water

427 jet. The impact of the broken wave on cylinder 2 results in a lower force for $S = 5D$ and
428 $6D$ and further increase in S would result in a lower force.

429 *Scenario D*

430 The total wave force on cylinder 1 in scenario D varies over a small range between $0.84F_0$ -
431 $0.90F_0$ in Fig. (14d). The peak wave force on cylinder 2 is the lowest for $S = 1D$ ($0.81F_0$)
432 and the highest for $S = 5D$ ($1.18F_0$). Due to the wave breaking just behind the upstream
433 cylinder 1, cylinder 2 is exposed to breaking wave impact and generally experiences higher
434 forces than cylinder 1. Similar to the previous scenarios where cylinder 2 is placed at a
435 distance of $S = 1D$, the incident wave crest is separated by cylinder 1, resulting in a lower
436 wave force on cylinder 2. From $S = 2D$ to $S = 5D$, cylinder 2 is impacted by the overturning
437 wave crest at and around the wave crest level as seen in Fig. (11c) for $S = 4D$, leading to
438 higher wave forces. The maximum peak force is calculated for $S = 5D$ where the breaker
439 tongue impacts cylinder 2 just below the wave crest level. On increasing S to $6D$, the
440 overturning wave crest rejoins the preceding wave trough during impact with cylinder 2 as
441 seen in Fig. (13c) and the wave force on cylinder 2 is reduced.

442 **Discussion**

443 The results show that the wave forces on both cylinders are generally less than the
444 wave force on a single cylinder in the same wave impact scenario (F_0). The exception to
445 this observation are the cases where the breaker tongue impacts the downstream cylinder
446 2 around the wave crest level. This is particularly the case in scenario D, where the wave
447 breaks behind the upstream cylinder 1 and the overturning wave crest impacts cylinder 2
448 around or just below wave crest level depending on the separation distance between the
449 cylinders. Another observation is that high runups are calculated on the second cylinder
450 when the cylinders are placed close to each other ($S = 1, 2D$), but the higher free surface
451 elevations do not correspond to higher wave forces. In fact, for scenarios C3, D4 and D6 the
452 free surface in front of cylinder 2 is lower than that in front of cylinder 1 whereas the wave
453 force is higher on cylinder 2. The close placement of the cylinders leads to a high runup from

454 the water jet developed in between the cylinders, but the second cylinder is shielded from
455 breaking wave impact due to the separation of the incident wavefront by the first cylinder.

456 The trend of the breaking wave forces on cylinder 1 for scenario B is seen to majorly
457 vary from the trend seen in the other scenarios for $S = 2D$ and $3D$. This is due to the
458 strong interaction between the incident waves and the waves reflected from the cylinder as
459 seen from previous studies by Hildebrandt et al. (2008) for cylinders placed close together.
460 In addition, the superposition of the reflected waves on the overturning wave crest is the
461 strongest as seen from Fig. (7a). This leads to a large increase followed by a large decrease
462 in the breaking wave forces for $S = 2D$ and $S = 3D$ respectively in this scenario. On further
463 increase in S , the breaking wave forces on cylinder 1 are around the values obtained for
464 $S = 1D$, which is the general trend in all the other scenarios.

465 Some similarities can be drawn between the results for wave forces on tandem cylinders
466 in this study and results for breaking wave forces on a single cylinder in previous studies.
467 In the case of a single cylinder, the maximum wave forces are obtained when the breaker
468 tongue impacts the cylinder just below the wave crest level (Irschik et al., 2002). In the
469 present study, the upstream cylinder 1 also experiences the highest forces in scenario A2
470 ($F = 13300N$) when the breaking impacts the cylinder just below wave crest level. In
471 scenario D4, cylinder 1 experiences one of the lowest forces ($F = 8330N$) when the wave
472 breaks just behind the cylinder. However, the lowest force on cylinder 1 is calculated in
473 scenario B3 ($F = 8174N$) due to the interaction between the incident and reflected waves
474 when the overturning wave crest impacts cylinder 1 at wave crest level.

475 For cylinder 2, the highest forces are calculated in scenario D5 ($F = 11564N$), when the
476 cylinder is placed at $S = 5D$ from cylinder 1 and the wave breaks just behind cylinder 1. The
477 overturning wave crest impacts cylinder 2 just below the wave crest level along with the water
478 jet. This is similar to the wave impact scenario leading to the highest breaking wave force on
479 a single cylinder. The lowest force on cylinder 2 ($F = 6300N$) is calculated in scenario A3,
480 where the overturning wave crest rejoins the preceding wave trough before impact with the

481 cylinder. Thus, the results from Wienke et al. (2000) and Irschik et al. (2002) for breaking
482 wave impact on a single slender cylinder are applicable in the case of tandem cylinder as
483 well, though with a few changes due to the interaction between the two cylinders placed in
484 proximity. The results in this study differ from the small-scale experimental results presented
485 by Apelt and Piorewicz (1986), which concluded that the separation between the cylinders
486 did not affect the wave forces on the cylinders when they are arranged in the direction of
487 wave propagation.

488 **CONCLUSIONS**

489 The open-source CFD model REEF3D is used to simulate plunging breaking wave in-
490 teraction with a pair of cylinders placed in tandem at different distances of separation for
491 different wave impact scenarios. The model was validated by comparing the numerical re-
492 sults for wave force and the free surface elevation with the experiments carried out on a
493 single cylinder at the Large Wave Flume, Hannover, Germany by Irschik et al. (2002). The
494 free surface features associated with breaking wave interaction with a slender cylinder are
495 presented and correlated to the wave forces on the cylinders and the following conclusions
496 can be drawn from the results:

- 497 • Similar to the results from wave impact on a single slender cylinder, the maximum
498 breaking wave forces in this study is calculated in cases where the breaker tongue
499 impacts the cylinders just below the wave crest level.
- 500 • The free surface features behind the first cylinder such as the separation of the wave-
501 front around the first cylinder, the formation of the water jet, the rejoining of the
502 separated wavefront and reconnection of the overturning wave crest with the preced-
503 ing wave trough have significant influence on the wave forces on the second cylinder.
504 The distance between the cylinders also determines the development of the various
505 free surface features.
- 506 • The wave forces on the first cylinder are lower than the force on a single cylinder for

507 the same wave impact scenario for all the cases studied. The highest force on the first
508 cylinder is $0.95F_0$ when the wave impacts the cylinder just below the wave crest level
509 and the second cylinder is at a distance of $2D$.

- 510 • The wave forces on the second cylinder are generally lower than the force on the first
511 cylinder when the wave breaks in front or at the first cylinder and the separation
512 distance is more than $4D$ with a highest force of $0.71F_0$ when the wave breaks exactly
513 at the first cylinder.
- 514 • The wave force on the second cylinder is higher than the force on the first cylinder and
515 the force on a single cylinder when the breaker tongue impacts the second cylinder
516 around the wave crest level. The highest force on the second cylinder is $1.18F_0$ when
517 the wave breaks just behind the first cylinder and the second cylinder is at a distance
518 of $5D$.

519 This study provides insight into the challenging problem of plunging breaking wave inter-
520 action with two cylinders in tandem for different wave impact scenarios and distances of
521 separation. Further studies can be carried out extended to investigate breaking wave in-
522 teraction with three or more cylinders in tandem, oblique wave incidence and engineering
523 problems including tripod substructures and coastal constructions with multiple cylinders
524 in proximity.

525 **ACKNOWLEDGEMENTS**

526 This study has been carried out under the OWCBW project (No. 217622/E20) and the
527 authors are grateful to the grants provided by the Research Council of Norway. This research
528 was supported in part with computational resources at the Norwegian University of Science
529 and Technology (NTNU) provided by NOTUR, <http://www.notur.no> (NN2620K).

530 **REFERENCES**

- 531 Alagan Chella, M., Bihs, H., and Myrhaug, D. (2015a). “Characteristics and profile asym-
532 metry properties of waves breaking over an impermeable submerged reef.” *Coastal Engi-
533 neering*, 100, 26–36.
- 534 Alagan Chella, M., Bihs, H., Myrhaug, D., and Muskulus, M. (2015b). “Breaking character-
535 istics and geometric properties of spilling breakers over slopes.” *Coastal Engineering*, 95,
536 4–19.
- 537 Alagan Chella, M., Tørum, A., and Myrhaug, D. (2012). “An overview of wave impact forces
538 on offshore wind turbine substructures.” *Energy Procedia*, 20, 217–226.
- 539 Apelt, C. J. and Piorewicz, J. (1986). “Interference effects on breaking wave forces on rows
540 of vertical cylinders.” *Proc. 1st Australasian Port, Harbour and Offshore Engineering
541 Conference, Sydney, Australia*.
- 542 Arntsen, Ø. A., Ros, X., and Tørum, A. (2011). “Impact forces on a vertical pile from
543 plunging breaking waves.” *Coastal Structures*.
- 544 Battjes, J. A. and Sakai, T. (1981). “Velocity field in a steady breaker.” *Journal of Fluid
545 Mechanics*, 111, 421–437.
- 546 Berthelsen, P. A. and Faltinsen, O. M. (2008). “A local directional ghost cell approach for
547 incompressible viscous flow problems with irregular boundaries.” *Journal of Computational
548 Physics*, 227, 4354–4397.
- 549 Blenkinsopp, C. E. and Chaplin, J. R. (2008). “The effect of crest submergence on wave
550 breaking over submerged slopes.” *Coastal Engineering*, 55, 967–974.
- 551 Bonmarin, P. (1989). “Geometric properties of deep-water breaking waves.” *Journal of Fluid
552 Mechanics*, 209, 405–433.
- 553 Bradford, S. F. (2000). “Numerical simulation of surf zone dynamics.” *Journal of Waterway,
554 Port, Coastal and Ocean Engineering*, 126, 1–13.

- 555 Bredmose, H. and Jacobsen, N. G. (2010). “Breaking wave impacts on offshore wind turbine
556 foundations: focused wave groups and CFD.” *Proc., 29th International Conference on*
557 *Ocean, Offshore and Arctic Engineering, Shanghai, China.*
- 558 Chan, E. S. and Melville, W. K. (1988). “Deep-water plunging wave pressures on a vertical
559 plane wall.” *Proc. of the Royal Society of London. A. Mathematical and Physical Sciences,*
560 *Vol. 417, 95–131.*
- 561 Chaplin, J. and Flinham, T., Greated, C., and Skyner, D. (1992). “Breaking wave forces on
562 a vertical cylinder.” *Report no.*, Health and Safety Executive, London, UK.
- 563 Chen, G., Kharif, C., Zaleski, S., and Li, J. (1999). “Two-dimensional Navier-Stokes simu-
564 lation of breaking waves.” *Physics of Fluids*, 11, 121–133.
- 565 Choi, S.-J., Lee, K.-H., and Gudmestad, O. T. (2015). “The effect of dynamic amplification
566 due to a structure s vibration on breaking wave impact.” *Ocean Engineering*, 96, 8–20.
- 567 Chorin, A. (1968). “Numerical solution of the Navier-Stokes equations.” *Mathematics of*
568 *Computation*, 22, 745–762.
- 569 Christensen, E. D. (1998). “Turbulence in breaking waves – a numerical investigation.” *PhD*
570 *thesis.*
- 571 Christensen, E. D. (2006). “Large eddy simulation of spilling and plunging breakers.” *Coastal*
572 *Engineering*, 53(5–6), 463–485.
- 573 Christensen, E. D. and Deigaard, R. (2001). “Large eddy simulation of breaking waves.”
574 *Coastal Engineering*, 42, 53–86.
- 575 Cokelet, E. D. (1977). “Breaking waves.” *Nature*, 267, 769–774.
- 576 Duncan, J. H. (2001). “Spilling breakers.” *Annual Review of Fluid Mechanics*, 33, 519–547.

- 577 Durbin, P. A. (2009). “Limiters and wall treatments in applied turbulence modeling.” *Fluid*
578 *Dynamics Research*, 41, 1–18.
- 579 Goda, Y., Haranaka, S., and Kitahata, M. (1966). “Study on impulsive breaking wave forces
580 on piles.” *Report Port and Harbour Technical Research Institute*, 6(5), 1–30.
- 581 Gourlay, M. R. (1994). “Wave transformation on a coral reef.” *Coastal Engineering*, 23,
582 17–42.
- 583 Hieu, P. D., Katsutoshi, T., and Ca, V. T. (2004). “Numerical simulation of breaking waves
584 using a two-phase flow model.” *Applied Mathematical Modeling*, 28(11), 983–1005.
- 585 Higuera, P., Lara, L. J., and Losada, I. J. (2013). “Realistic wave generation and active wave
586 absorption for Navier-Stokes models application to OpenFOAM.” *Coastal Engineering*, 71,
587 102–118.
- 588 Hildebrandt, A. and Schlurmann, T. (2012). “Breaking wave kinematics, local pressures,
589 and forces on a tripod structure.” *Coastal Engineering*, Vol. 1, 71.
- 590 Hildebrandt, A., Sparboom, U., and Oumeraci, H. (2008). “Wave forces on groups of slen-
591 der cylinders in comparison to an isolated cylinder due to non-breaking waves.” *Coastal*
592 *Engineering*, 3770–3781.
- 593 Irschik, K., Sparboom, U., and Oumeraci, H. (2002). “Breaking wave characteristics for the
594 loading of a slender pile.” *Proc. 28th International Conference on Coastal Engineering*,
595 *Cardiff, Wales*.
- 596 Jacobsen, N. G., Fuhrman, D. R., and Fredsøe, J. (2012). “A wave generation toolbox for
597 the open-source CFD library: OpenFOAM.” *International Journal for Numerical Methods*
598 *in Fluids*, 70(9), 1073–1088.
- 599 Jiang, G. S. and Peng, D. (2000). “Weighted ENO schemes for Hamilton-Jacobi equations.”
600 *SIAM Journal on Scientific Computing*, 21, 2126–2143.

601 Jiang, G. S. and Shu, C. W. (1996). “Efficient implementation of weighted ENO schemes.”
602 *Journal of Computational Physics*, 126, 202–228.

603 Kamath, A., Alagan Chella, M., Bihs, H., and Arntsen, Ø. A. (2015). “Cfd investigations of
604 wave interaction with a pair of large tandem cylinders.” *Ocean Engineering*, 108, 738–748.

605 Kjeldsen, S. and Myrhaug, D. (1978). *Kinematics and dynamics of breaking waves*. River
606 and Harbour Laboratory (NHL) The Norwegian Institute of Technology.

607 Larsen, J. and Dancy, H. (1983). “Open boundaries in short wave simulations - a new
608 approach.” *Coastal Engineering*, 7, 285–297.

609 Lin, P. and Liu, P. L. F. (1998). “A numerical study of breaking waves in the surf zone.”
610 *Journal of Fluid Mechanics*, 359, 239–264.

611 Miller, R. L. (1987). “Role of vortices in surf zone prediction: sedimentation and wave
612 forces.” *The Society of Economic Paleontologists and Mineralogists, Special Publications*,
613 (24), 92–114.

614 Mo, W., Jensen, A., and Liu, P. L. F. (2013). “Plunging solitary wave and its interaction
615 with a slender cylinder on a sloping beach.” *Ocean Engineering*, 74, 48–60.

616 Morison, J. R., O’Brien, M. P., Johnson, J. W., and Schaaf, S. A. (1950). “Force exerted by
617 surface waves on piles.” *Journal of Petroleum Technology*, 2, 149–154.

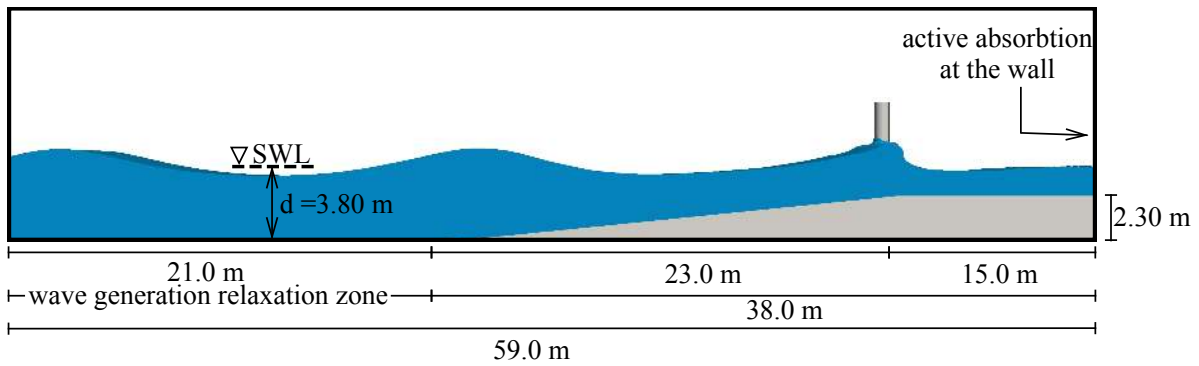
618 Nadaoka, K., Hino, M., and Koyano, Y. (1989). “Structure of the turbulent flow field under
619 breaking waves in the surf zone.” *Journal of Fluid Mechanics*, 204, 359–387.

620 Naot, D. and Rodi, W. (1982). “Calculation of secondary currents in channel flow.” *Journal*
621 *of the Hydraulic Division, ASCE*, 108(8), 948–968.

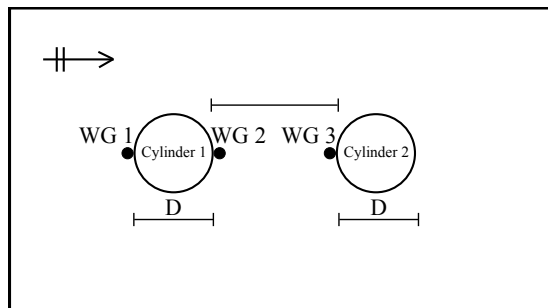
622 Osher, S. and Sethian, J. A. (1988). “Fronts propagating with curvature- dependent speed:
623 algorithms based on Hamilton-Jacobi formulations.” *Journal of Computational Physics*,
624 79, 12–49.

- 625 Peng, D., Merriman, B., Osher, S., Zhao, H., and Kang, M. (1999). “A PDE-based fast local
626 level set method.” *Journal of Computational Physics*, 155, 410–438.
- 627 Rapp, R. J. and Melville, W. K. (1990). “Laboratory measurements of deep-water break-
628 ing waves.” *Philosophical Transactions of the Royal Society of London A: Mathematical,*
629 *Physical and Engineering Sciences*, 331(1622), 735–800.
- 630 Sawaragi, T. and Nochino, M. (1984). “Impact forces of nearly breaking waves on a vertical
631 circular cylinder.” *Coastal Engineering in Japan*, 27, 249–263.
- 632 Schäffer, H. A. and Klopman, G. (2000). “Review of multidirectional active wave absorption
633 methods.” *Journal of Waterway, Port, Coastal, and Ocean Engineering*, 126(2), 88–97.
- 634 Shu, C. W. and Osher, S. (1988). “Efficient implementation of essentially non-oscillatory
635 shock capturing schemes.” *Journal of Computational Physics*, 77, 439–471.
- 636 Smith, E. R. and Kraus, N. C. (1990). “Laboratory study on macro-features of wave breaking
637 over bars and artificial reefs.” *Report no.*, Coastal Engineering Research Center.
- 638 Sparboom, U., Hildebrandt, A., and Oumeraci, H. (2006). “Group interaction effects of
639 slender cylinders under wave attack.” *Coastal Engineering*, 4430–4442.
- 640 Sparboom, U., Oumeraci, H., Schmidt-Koppenhagen, R., and Grüne, J. (2005). “Large-scale
641 model study on cylinder groups subject to breaking and nonbreaking waves.” *Proc. 5th*
642 *International Symposium WAVES 2005 Ocean Waves Measurement and Analysis, Madrid,*
643 *Spain.*
- 644 Stive, M. J. F. and Wind, H. G. (1982). “A study of radiation stress and set-up in the
645 nearshore region.” *Coastal Engineering*, 6, 1–26.
- 646 Ting, F. C. K. and Kim, Y. K. (1994). “Vortex generation in water waves propagating over
647 a submerged obstacle.” *Coastal Engineering*, 24(1), 23–49.

- 648 van der Vorst, H. (1992). “BiCGStab: A fast and smoothly converging variant of Bi-CG for
649 the solution of nonsymmetric linear systems.” *SIAM Journal on Scientific and Statistical*
650 *Computing*, 13, 631–644.
- 651 Wang, Z., Zou, Q., and Reeve, D. (2009). “Simulation of spilling breaking waves using a two
652 phase flow CFD model.” *Computers and Fluids*, 38(10), 1995–2005.
- 653 Watanbe, A. and Horikawa, K. (1974). “Breaking wave forces on a large diameter cell.”
654 *Coastal Engineering Proceedings*, 1(14).
- 655 Wienke, J. and Oumeraci, H. (2005). “Breaking wave impact force on a vertical and inclined
656 slender pile – theoretical and large-scale model investigations.” *Coastal Engineering*, 52,
657 435–462.
- 658 Wienke, J., Sparboom, U., and Oumeraci, H. (2000). “Breaking wave impact on a slender
659 cylinder.” *Coastal Engineering Conference*, Vol. 2, 1787–1798.
- 660 Wilcox, D. C. (1994). *Turbulence modeling for CFD*. DCW Industries Inc., La Canada,
661 California.
- 662 Xie, Z. (2013). “Two-phase flow modelling of spilling and plunging breaking waves.” *Applied*
663 *Mathematical Modelling*, 37, 3698–3713.
- 664 Zhao, Q., Armfield, S., and Tanimoto, K. (2004). “Numerical simulation of breaking waves
665 by a multi-scale turbulence model.” *Coastal Engineering*, 51(1), 53–80.

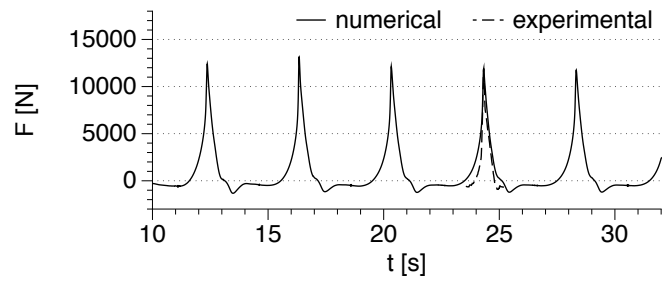


(a) numerical wave tank showing the dimensions of the tank and wave generation and absorption zones

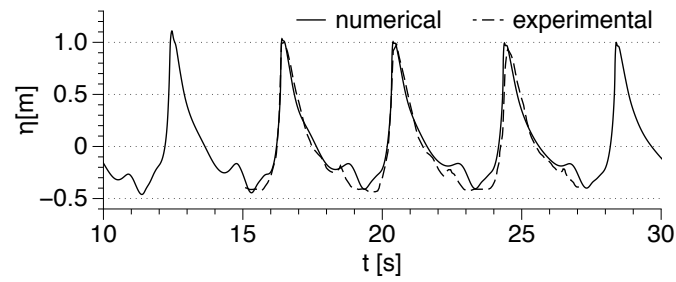


(b) schematic diagram showing the wave gage locations around the cylinders

Fig. 1. Numerical wave tank setup used in the study



(a) wave force on the cylinder



(b) free surface near the wall along the frontline of the cylinder

Fig. 2. Comparison of the numerical and experimental results

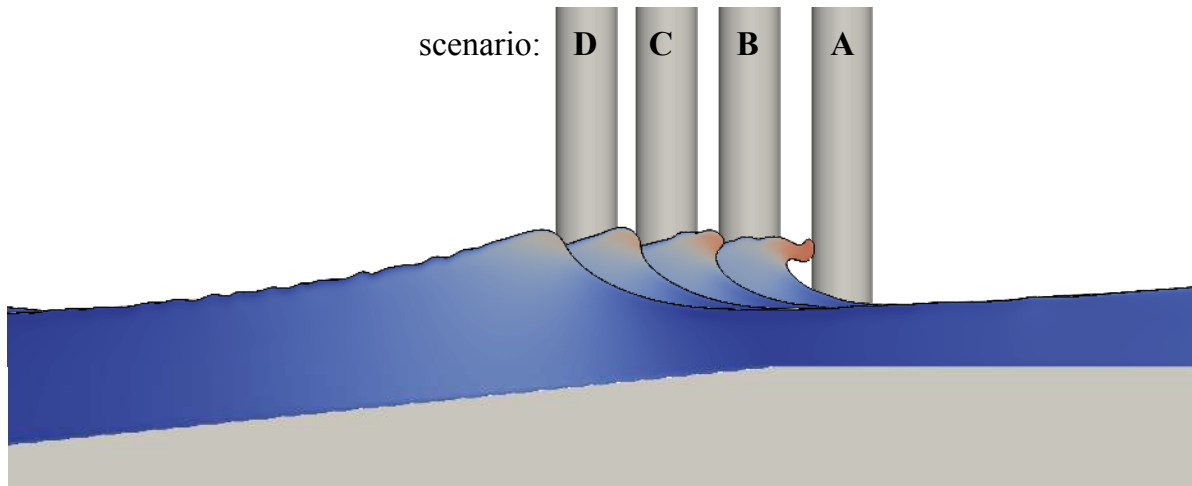
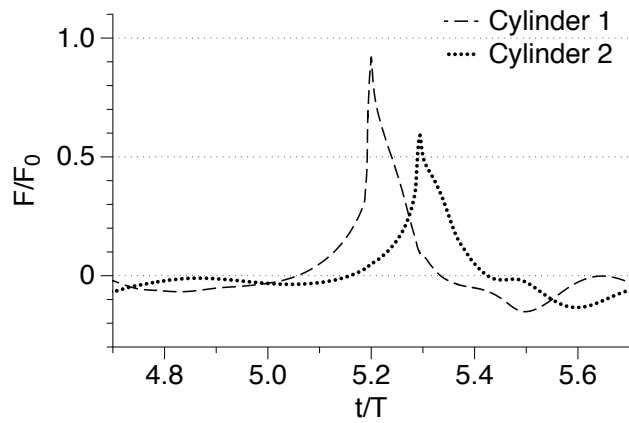
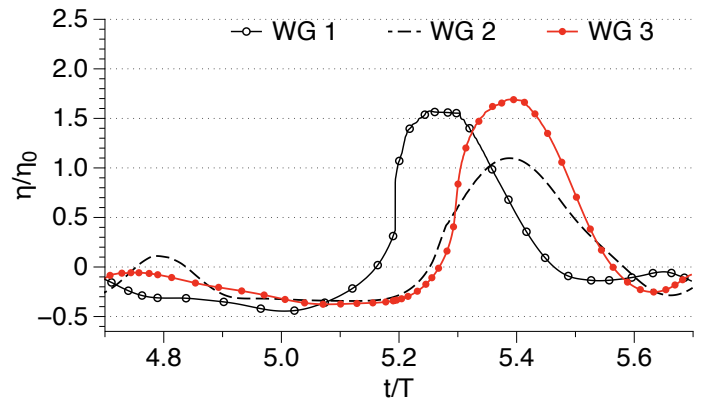


Fig. 3. Four different locations of cylinder 1 with respect to the wave breaking point considered in the study



(a) breaking wave forces on the cylinders



(b) free surface elevations around the cylinders

Fig. 4. Wave forces on and free surface elevations around the cylinders for scenario A1: breaker tongue impacting cylinder just below wave crest level with $S = 1D$

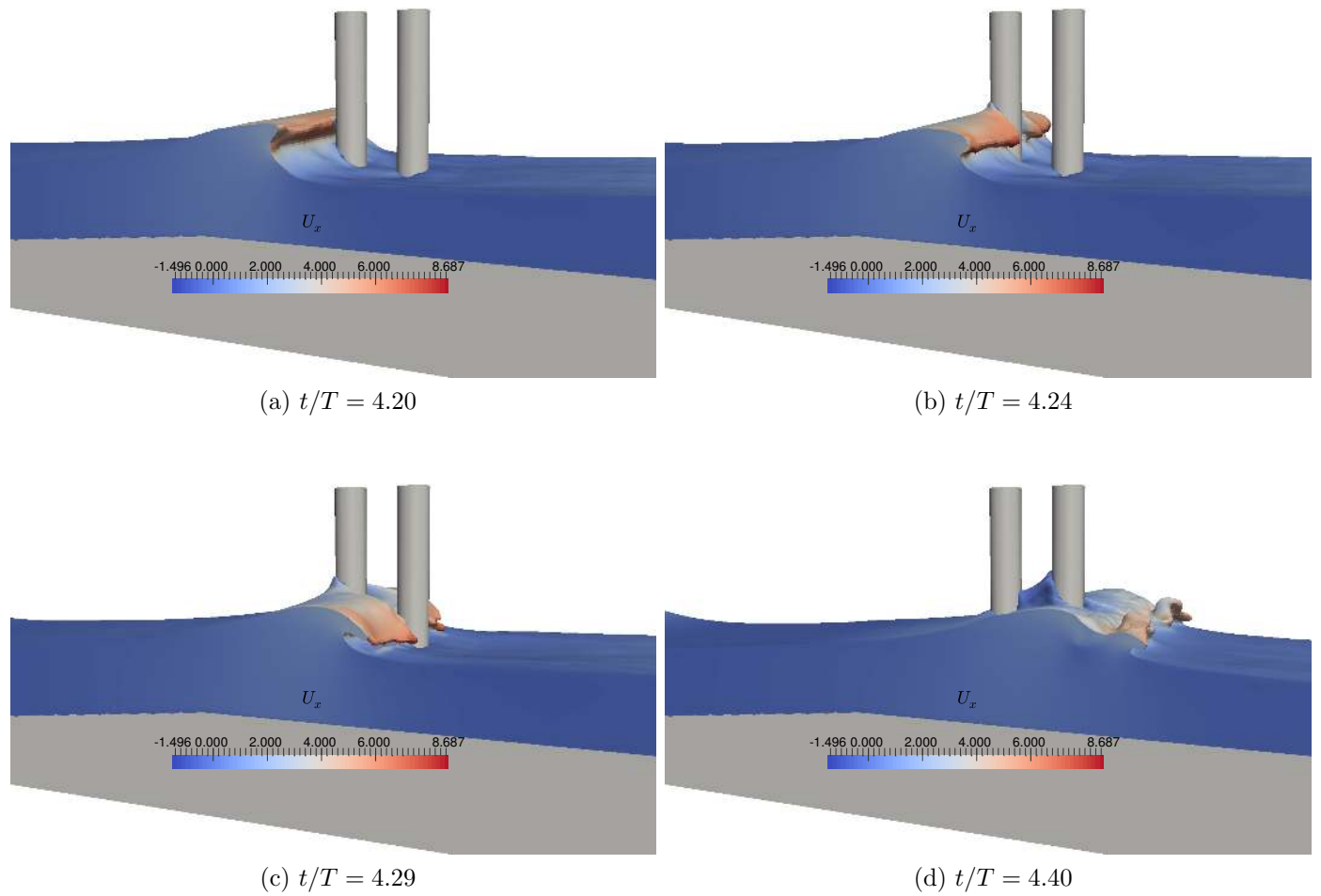
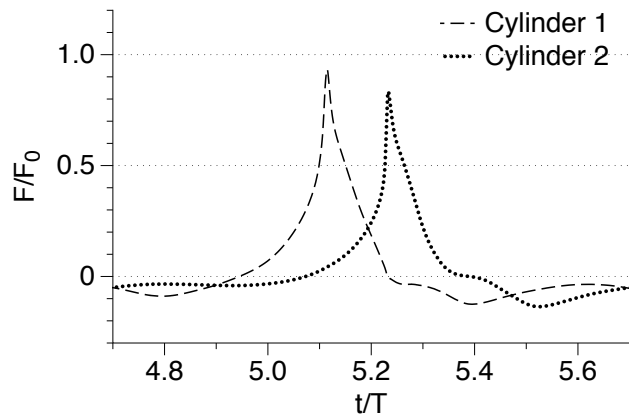
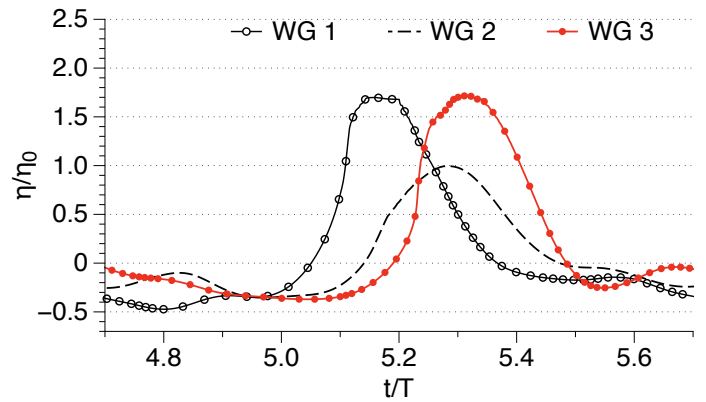


Fig. 5. Free surface around the cylinders in scenario A1 ($S = 1D$) with horizontal velocity contours

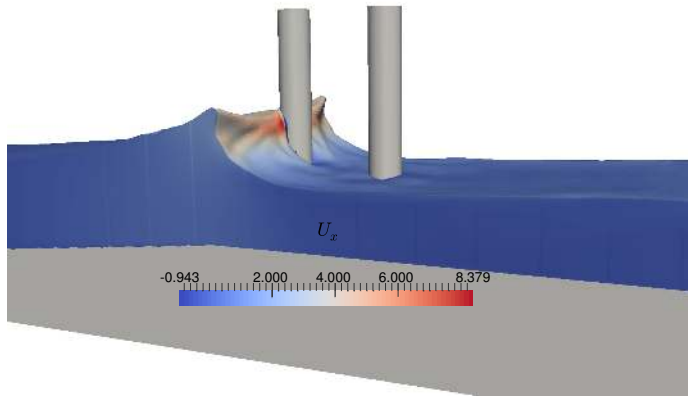


(a) breaking wave forces on the cylinders

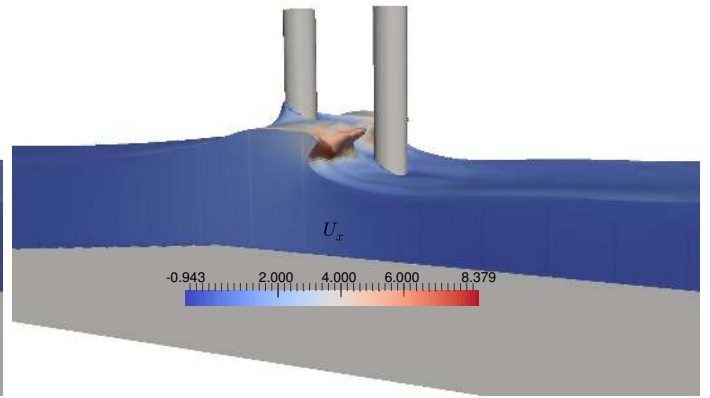


(b) free surface elevations around the cylinders

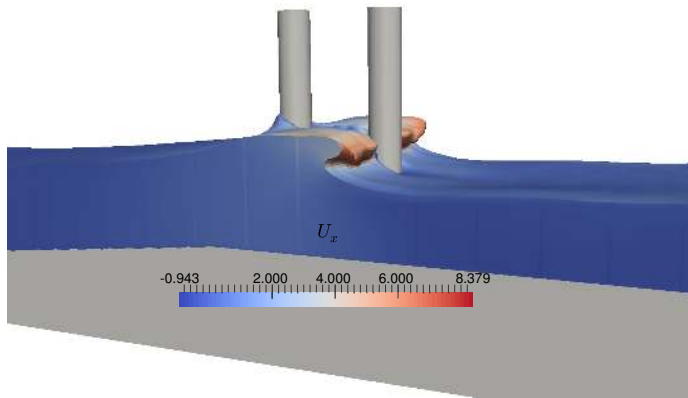
Fig. 6. Wave forces on and free surface elevations around the cylinders for scenario B2: breaker tongue impacting cylinder at wave crest level with $S = 2D$



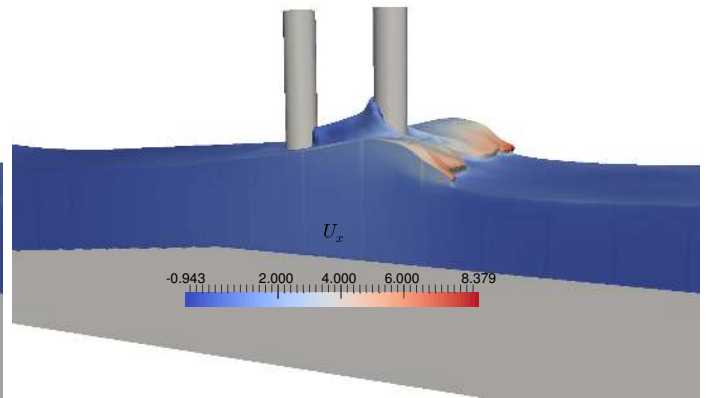
(a) $t/T = 4.11$



(b) $t/T = 4.20$

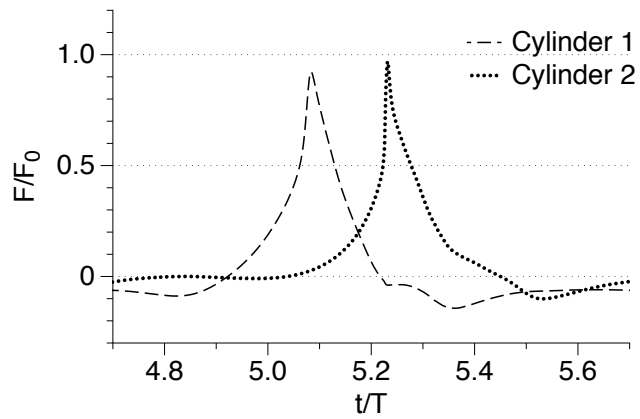


(c) $t/T = 4.23$

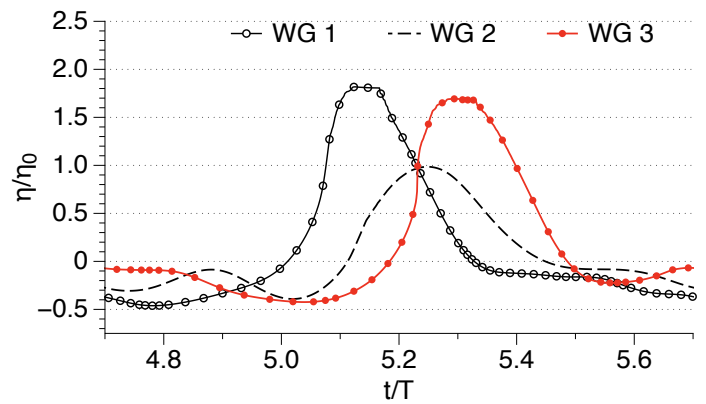


(d) $t/T = 4.31$

Fig. 7. Free surface around the cylinders in scenario B2 ($S = 2D$) with horizontal velocity contours

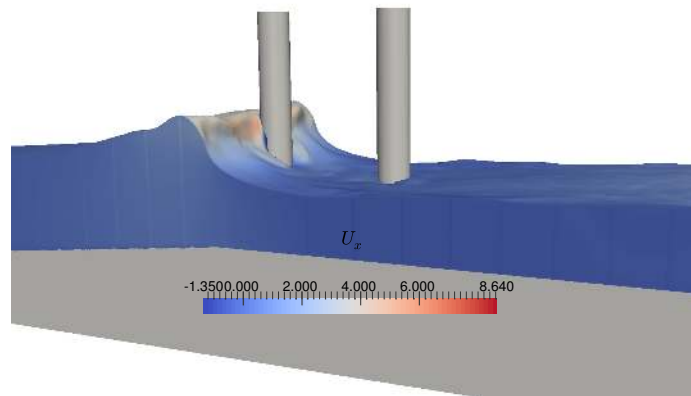


(a) breaking wave forces on the cylinders

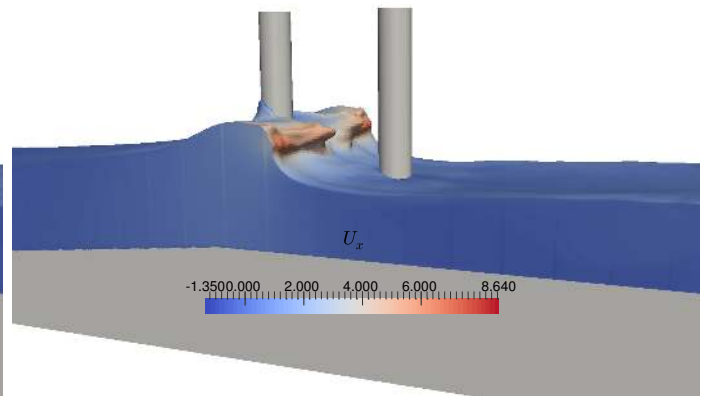


(b) free surface elevations around the cylinders

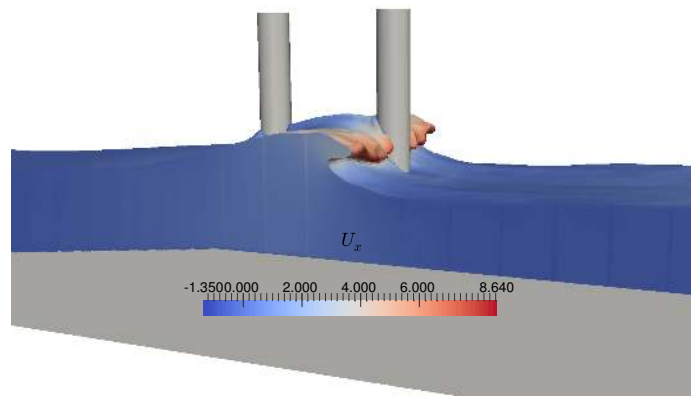
Fig. 8. Wave forces on and free surface elevations around the cylinders for scenario C3: wave breaking exactly at the first cylinder with $S = 3D$



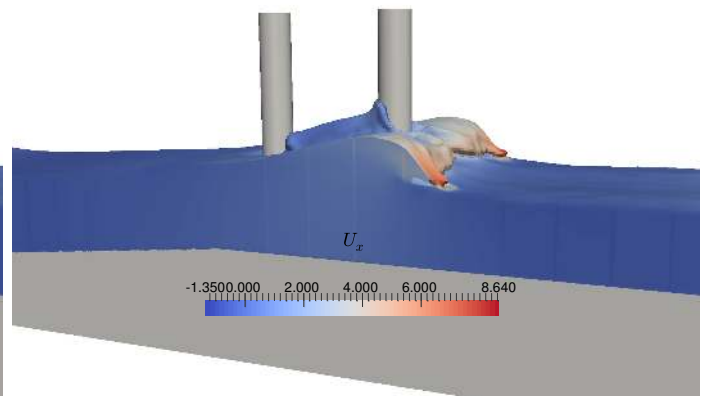
(a) $t/T = 4.08$



(b) $t/T = 4.18$

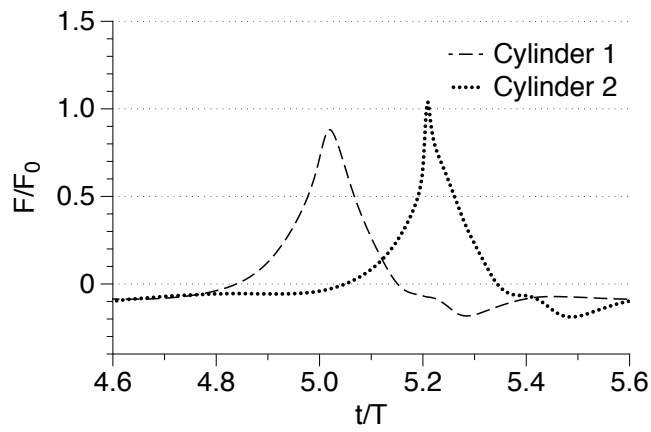


(c) $t/T = 4.25$

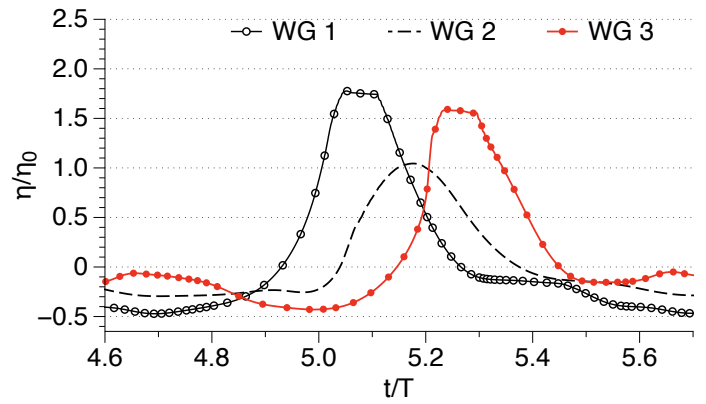


(d) $t/T = 4.32$

Fig. 9. Free surface around the cylinders in scenario C3 ($S = 3D$) with horizontal velocity contours



(a) breaking wave forces on the cylinders



(b) free surface elevations around the cylinders

Fig. 10. Wave forces on and free surface elevations around the cylinders for scenario D4: wave breaking just behind the first cylinder with $S = 4D$

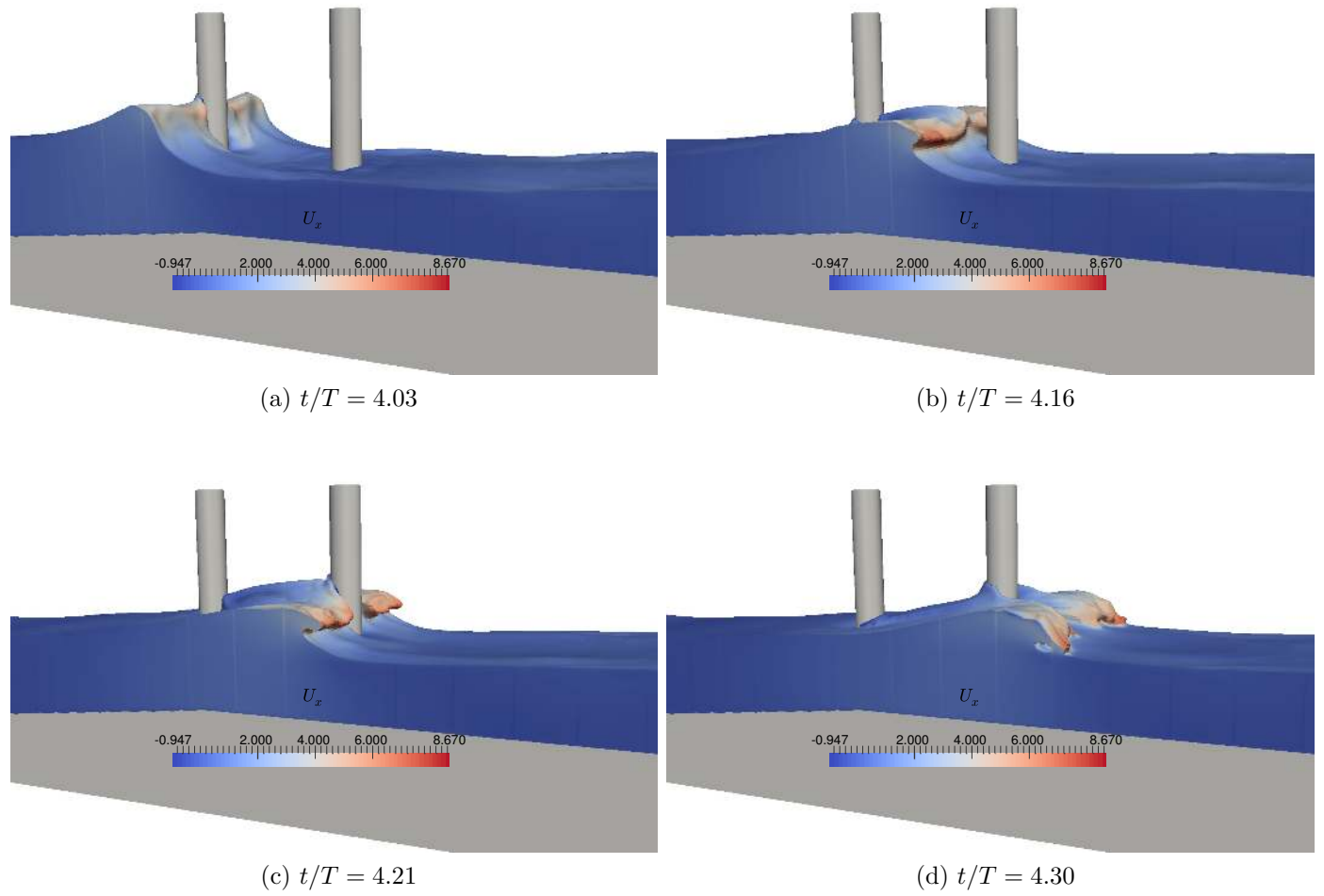
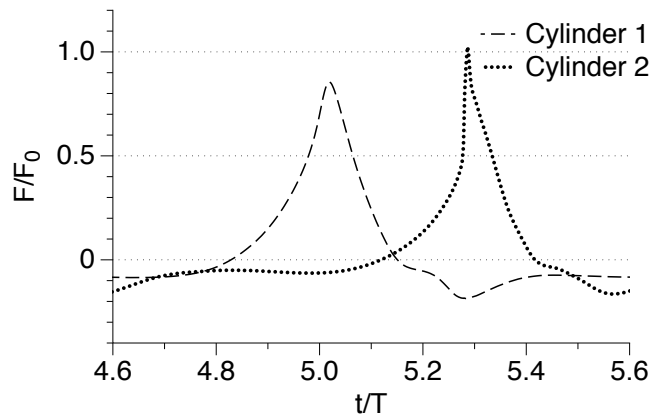
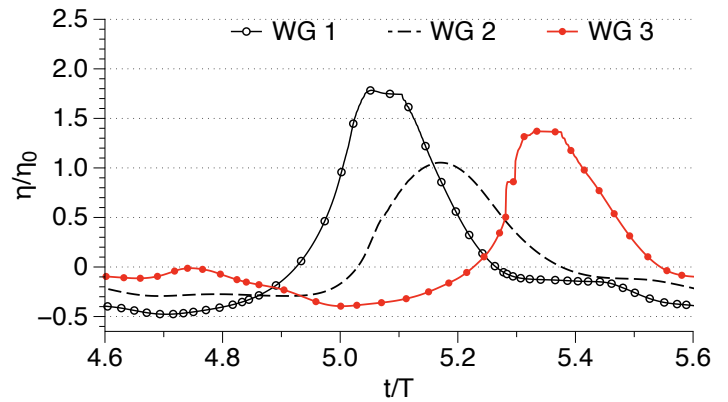


Fig. 11. Free surface around the cylinders in scenario D4 ($S = 4D$) with horizontal velocity contours



(a) breaking wave forces on the cylinders



(b) free surface elevations around the cylinders

Fig. 12. Wave forces on and free surface elevations around the cylinders for scenario D6: wave breaking just behind the first cylinder with $S = 6D$

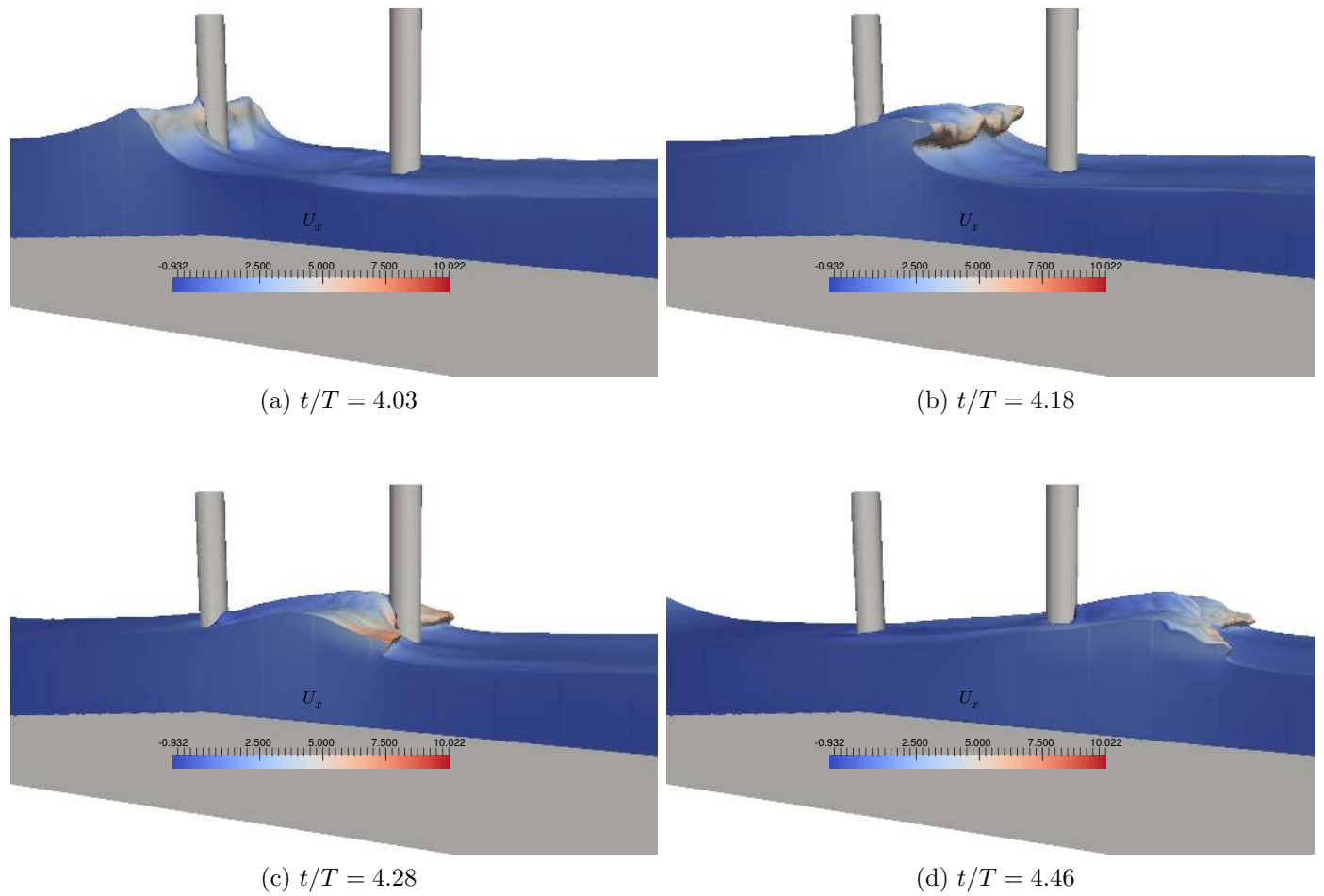
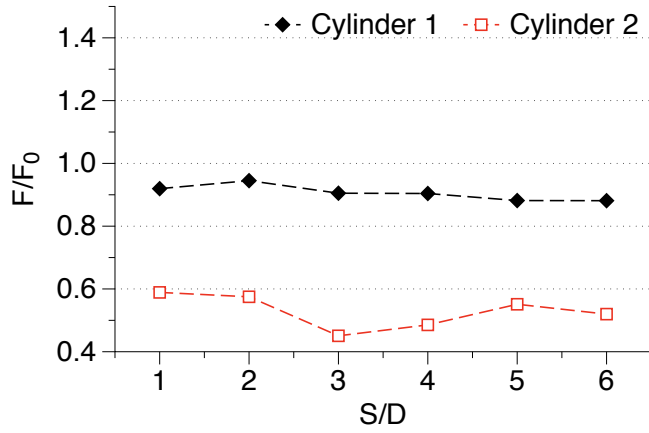
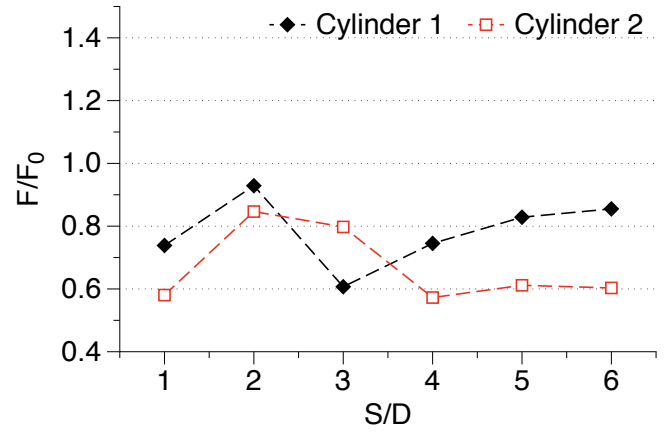


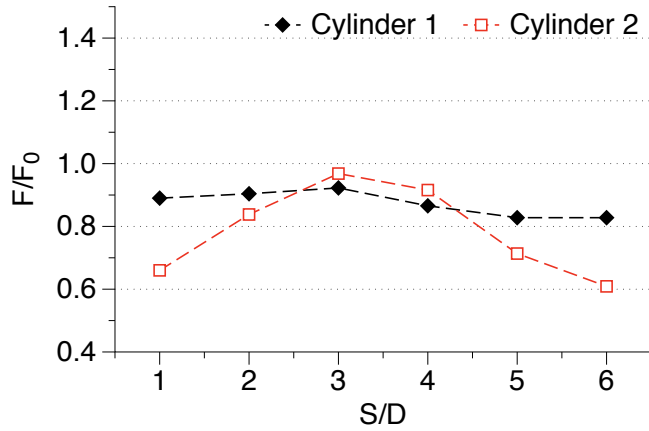
Fig. 13. Free surface around the cylinders in scenario D6 ($S = 6D$) with horizontal velocity contours



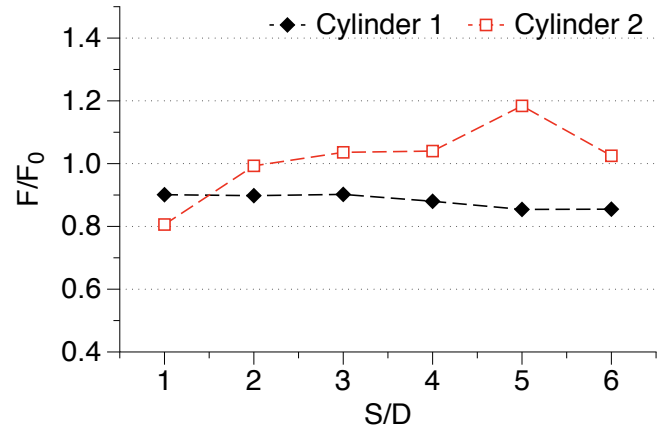
(a) scenario A: breaker tongue impact on cylinder 1 just below wave crest level



(b) scenario B: breaker tongue impact on cylinder 1 at wave crest level



(c) scenario C: wave breaking exactly at cylinder 1



(d) scenario D: wave breaking just behind cylinder 1

Fig. 14. Variation of the maximum wave force on the cylinders with distance of separation S in different wave impact scenarios

Table 1. Details of the setups used in the different simulations

Case	H (m)	T (s)	S (m)	scenario	F_0 (N)	F_1/F_0	F_2/F_0	η_{cyl1}/η_0	η_{cyl2}/η_0
A1	1.30	4.00	1D	overturning	14000	0.92	0.59	1.58	1.69
A2			2D	wave crest		0.95	0.58	1.64	1.75
A3			3D	impact on		0.91	0.45	1.57	1.58
A4			4D	cylinder 1 just		0.90	0.48	1.56	1.62
A5			5D	below wave		0.88	0.55	1.59	1.70
A6			6D	crest level		0.88	0.52	1.68	1.58
B1	1.30	4.00	1D	overturning	13400	0.74	0.58	1.76	1.71
B2			2D	wave crest		0.93	0.85	1.70	1.72
B3			3D	impact on		0.61	0.80	1.75	1.58
B4			4D	cylinder 1 at		0.75	0.57	1.69	1.56
B5			5D	wave crest level		0.83	0.61	1.69	1.45
B6			6D			0.86	0.60	1.70	1.37
C1	1.30	4.00	1D	wave breaking exactly at cylinder 1	11850	0.89	0.66	1.82	1.77
C2			2D			0.90	0.84	1.70	1.84
C3			3D			0.92	0.97	1.82	1.70
C4			4D			0.86	0.92	1.76	1.63
C5			5D			0.83	0.71	1.70	1.44
C6			6D			0.83	0.61	1.76	1.32
D1	1.30	4.00	1D	wave breaking just behind cylinder 1	9800	0.90	0.81	1.83	1.79
D2			2D			0.89	0.99	1.94	1.89
D3			3D			0.90	1.03	1.70	1.76
D4			4D			0.88	1.04	1.78	1.59
D5			5D			0.85	1.18	1.83	1.45
D6			6D			0.85	1.02	1.78	1.37